ACS OMEGA

Article

Cite This: ACS Omega 2017, 2, 8836−8842

Magnetic and Electrical Performance of Atomic Layer Deposited Iron Erbium Oxide Thin Films

Aile Tamm,*[,†] Kristjan Kalam,[†] Helina Seemen,[†] Jekaterina Kozlova,[†] Kaupo Kukli,[†,‡] Jaan Aarik,[†] Joosep Link,[§] Raivo Stern,[§] Salvador Dueñas,[∥] and Helena Castán[∥]

[†]Institute of Physics, University of Tartu, W. Ostwaldi 1, 50411 Tartu, Estonia

[‡]Department of Chemistry, University of Helsinki, P.O. Box 55, FI-00014 Helsinki, Finland

[§]National Institute of Chemical Physics and Biophysics, Akadeemia tee 23, 12618 Tallinn, Estonia

[∥]Department of Electronics, University of Valladolid, Paseo Belén, 15, 47011 Valladolid, Spain

ABSTRACT: Mixed films of a high-permittivity oxide, Er_2O_3, and a magnetic material, Fe_2O_3, were grown by atomic layer deposition on silicon and titanium nitride at 375 °C using erbium diketonate, ferrocene, and ozone as precursors. Crystalline phases of erbium and iron oxides were formed. Growth into three-dimensional trenched structures was demonstrated. A structure deposited using tens to hundreds subsequent cycles for both constituent metal oxide layers promoted both charge polarization and saturative magnetization compared to those in the more homogeneously mixed films.

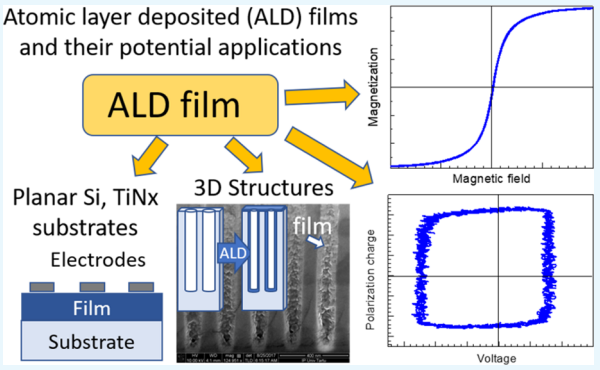

INTRODUCTION

Mixtures of rare earth ferrites have been of interest due to their attractive optical, electrical, and magnetic properties. Herewith some hexagonal orthoferrites $RFeO_3$, where R denotes a trivalent rare earth cation, such as epitaxial $YbFeO_3$[1] or single-crystal $LuFeO_3$,[2] have been described as materials demonstrating recordable ferroelectric polarization. The latter ternary materials have also been defined as multiferroic. Further, in epitaxially grown rare earth ferrite materials, weak ferromagnetism at low temperatures has been recorded, e.g., in the case of erbium ferrite below 120 K.[3] Moreover, polarization in both external electric and magnetic fields at room temperature has been recorded in pulsed laser deposited hexagonally structured $ErFeO_3$ films,[4,5] revealing polarization-charge-field loops characteristic of ferroelectric polarization, as claimed, and also narrow magnetization-field hysteresis loops.

Physical performance of the materials layers may considerably depend on their synthesis routes. The materials grown epitaxially or using precursor materials of the highest purity, such as those mentioned above, may exhibit structural and chemical qualities relatively close to the perfection. At the same time, thin solid films or particles deposited on substrates not supporting commensurate growth, or synthesized chemically in low-temperature processes exploiting precursors with ligands, will inevitably contain large amounts of residual contaminants and/or possess disordered polycrystalline structure. In such materials, the achievement of well-defined physical performance and appearance of functionality may easily occur complicated. For instance, particles of different rare earth oxides, including $ErFeO_3$, obtained by sonochemical method from $Fe(CO)_5$ and rare earth carbonate precursors, exhibited almost insignificant magnetization hysteresis at room temperature.[6] Deteriorating effect on the magnetic coercivity of secondary phases and concurrent reversed domains appearing upon increase in the growth rate was demonstrated in the case of otherwise single-crystal $ErFeO_3$ grown by the floating-zone method.[7]

Synthesis of thin erbium ferrite films at low temperatures, possessing defined electric and magnetic properties, is thus presumably challenging and has been attempted scarcely. Iron erbium oxide (Er−Fe−O) thin films have been grown earlier by atomic layer deposition (ALD) using either a cyclopentadienyl-type precursor for erbium, carbonyl-type precursor for iron, and ozone for oxygen[8] or β-diketonates of erbium and iron, and ozone.[9] The material to be magnetized has been grown initially in the form of a double layer,[8] comprising a 9 nm thick Er_2O_3 deposited at 200 °C, followed by the deposition of 14 nm thick FeO_x at 350 °C. The stack was subsequently annealed and recrystallized as ternary solids, e.g., $ErFeO_3$, $ErFe_2O_4$, and $Er_3Fe_5O_{12}$, evidently after solid-state reaction at 850 °C. The appearance of certain ferromagnetic moment in the film at room temperature was recorded.[8] These films were not yet characterized electrically.

In the present study, the thin films containing iron and erbium oxides were grown by atomic layer deposition using

Received: September 19, 2017
Accepted: November 27, 2017
Published: December 11, 2017

DOI: 10.1021/acsomega.7b01394
ACS Omega 2017, 2, 8836−8842

Table 1. Growth Cycle Ratios, Er/Fe Atomic Ratios Determined by X-ray Fluorescence (XRF), and Thicknesses, Measured with Spectroscopic Ellipsometry, of Er_2O_3:Fe_2O_3 Films Deposited on Planar SiO_2/Si Substrates

cycle ratio notation	growth cycle sequence	Er/Fe cation ratio	thickness on Si (nm)
(1:1)	$500 \times (1 \times Er_2O_3 + 1 \times Fe_2O_3)$	<0.002	65.1 ± 0.1
(3:1)	$200 \times (3 \times Er_2O_3 + 1 \times Fe_2O_3)$	0.02	56.6 ± 0.1
(60:3)	$20 \times (60 \times Er_2O_3 + 3 \times Fe_2O_3)$	0.46	5.2 ± 0.1
(50:5)	$22 \times (50 \times Er_2O_3 + 5 \times Fe_2O_3)$	0.30	19.5 ± 0.1
(50:1)	$20 \times (50 \times Er_2O_3 + 1 \times Fe_2O_3)$	0.26	14.9 ± 0.2
(300:20)	$2 \times (300 \times Er_2O_3 + 20 \times Fe_2O_3) + 300 \times Er_2O_3$	0.18	5.7 ± 0.1

tris(2,2,6,6-tetramethyl-3,5-heptanedionato)erbium ($Er(thd)_3$) and $Fe(C_5H_5)_2$ ($FeCp_2$) as metal precursors, and O_3 as an oxygen precursor. The films were grown both mixtures and laminate-like stacks of iron and erbium oxides using sequential deposition of just a few layers for constituent oxides, or using tens of cycles for every separate layer of erbium and iron oxides. Composition, structure, and magnetic and electrical behavior of the films were examined.

RESULTS AND DISCUSSION

Film Growth, Morphology, and Structure. On planar SiO_2/Si substrates, the Er_2O_3 and Fe_2O_3 reference films were grown to the thicknesses of 4.0 ± 0.5 and 20.9 ± 0.1 nm after 1000 growth cycles, respectively. Thus, the average growth rates of constituent oxides separately were 0.004 and 0.021 nm/cycle for Er_2O_3 and Fe_2O_3 films, respectively. One can note marked differences in the film growth, evidently affected by the choice of reactor conditions, including growth temperature, oxidizing agents, and deposition cycle time parameters. In an earlier study devoted to ALD of Fe_2O_3 from $FeCp_2$ and O_3, the growth rates reaching 0.09−0.12 nm/cycle were measured.[10] In this study, however, the metal precursor and ozone pulse lengths were extended to truly high values, over 40 and 200 s, to achieve saturation in growth rate versus precursor pulse length dependences. The growth temperature was also rather low, 200 °C. Yet, in another process, where very short precursor pulses, i.e., 2 s for ferrocene and only 0.2 s for ozone,[11] were used, the growth rate of iron oxide was 0.022 nm/cycle at 200−220 °C, which is well comparable to the rate observed in our present study. Somewhat surprisingly, the growth rates of the Fe_2O_3 films registered in the present study are inferior to those observed earlier in an ALD process using $FeCp_2$ and oxygen as Fe_2O_3 precursors under analogous conditions.[12] In the latter study, where the ferrocene and oxygen pulse lengths were 3 and 7 s, respectively, Fe_2O_3 films grew with the rate of 0.14 nm/cycle at temperatures comparable to that applied in the present study. By contrast, a growth per cycle of 0.03−0.04 nm has been obtained for the $FeCp_2$−O_3 process at 400 °C.[13] Most importantly, it has been revealed that the incubation time that depends on substrate pretreatment might exceed even 200 cycles in this ALD process on the SiO_2/Si substrates.[13] This explains why the growth rates obtained in different experiments and for different kind of structures differ significantly. For instance, the growth rate 0.1 nm per cycle was obtained for the Fe_2O_3 sublayers deposited in the present work by applying 20 $FeCp_2$−O_3 cycles after 300 $Er(thd)_3$−O_3 cycles (Table 1). Earlier also, the Er_2O_3 films have been grown with a higher rate, 0.235 nm/cycle, from $Er(thd)_3$ and O_3 precursors at 300 °C.[14] In the latter study, a deposition reactor enabling higher gas flow rates were exploited, and 2.5 s long ozone pulses after 1.25 s long metal precursor pulses were applied. Thus, depending on the reactor conditions and the choice of cycle time parameters, certain diversity appears concerning the growth rate of the target material. In the case of multicomponent materials, one has to consider the experimental results characteristic of a particular setup, taking into account the largest variations expected to occur during the first deposition cycles of one oxide onto another.

The marked difference in the growth rates of constituent oxides later necessitated the application of much higher amounts of Er_2O_3 growth cycles, compared to those for Fe_2O_3 to deposit multilayer-like structures consisting of distinctive Er_2O_3 and Fe_2O_3 layers. The X-ray fluorescence (XRF) analysis revealed that the cycle ratio of 50:5 or 60:3 resulted in the highest Er/Fe atomic ratios, which were still markedly lower than that for the stoichiometric erbium ferrite $ErFeO_3$ (Table 1). One should consider that, in the case of ALD, few deposition cycles, such as 1−5 applied here for the growth of each Fe_2O_3 layer, do not suffice for the formation of chemically and structurally defined single metal oxide, but result in the growth of a discontinuous submonolayer of metal oxide. As a consequence, this should result in a mixture of oxides rather than a multilayer structure. Further, taking into account that tens of erbium oxide deposition cycles applied between iron oxide deposition cycles resulted in films containing more than 2 times lower amounts of erbium compared to iron, the films deposited cannot be regarded as nanolaminates (multilayers) but rather the mixtures of two different metal oxides. In the case of relatively low amounts of Er_2O_3 applied, the films may even be regarded as those of erbium (oxide) doped iron oxides.

Scanning electron microscopy (SEM) images demonstrated that the surfaces of Er_2O_3:Fe_2O_3 films were quite smooth without significant features referring to a polycrystalline structure (Figure 1). The morphology of the films obviously depended somewhat on the growth recipe. High relative amounts of Er_2O_3 growth cycles (Er_2O_3:Fe_2O_3 cycle ratios of 60:3 and 50:1) resulted in amorphous and, consequently, smoother films compared to those grown using low amounts of Er_2O_3 growth cycles (1:1). The bird-eye SEM images visually implied certain tiny grainlike features on the surface of the films grown using cycle ratios 50:1 and 50:5. These are not, however, to be taken as direct indications of the crystal growth, but rather small-sized agglomerations of disordered material often visible on the images taken from X-ray amorphous film surfaces. As will later be seen from the X-ray diffraction (XRD) data, the crystal structure is not fully formed in these films. It should also be taken into account, that the film thicknesses are not to be necessarily and directly compared to each other based just on the numbers of constituent oxide cycles because the nucleation delays for the constituents and their corresponding growth rates at the early growth stages may differ considerably. The detailed and, thus, extensive studies of these effects remained beyond the scope of this work. However, an amorphous film

DOI: 10.1021/acsomega.7b01394
ACS Omega 2017, 2, 8836−8842

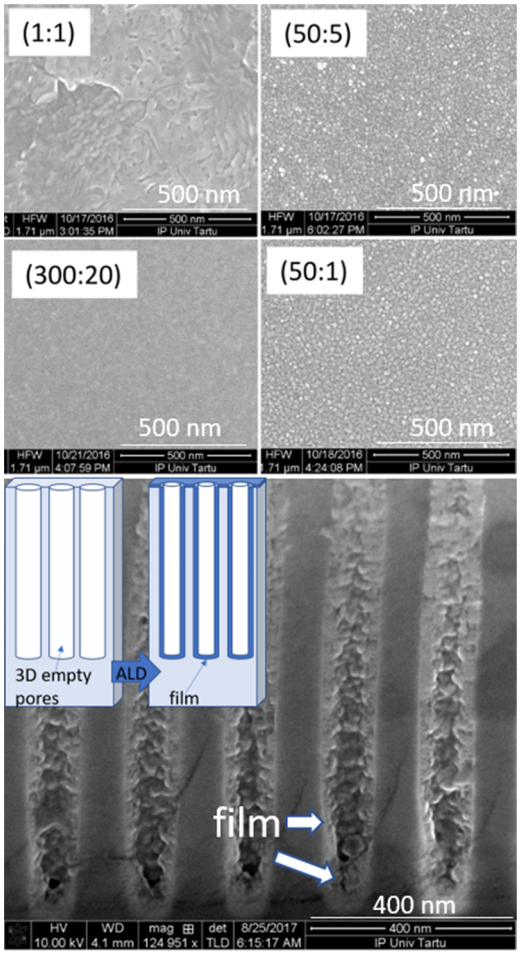

Figure 1. Bird-eye scanning electron microscopy images of as-deposited Er_2O_3:Fe_2O_3 films with cycle ratios of 1:1, 50:5, 50:1, and 300:20, indicated by labels, and cross-sectional image of the as-deposited Er_2O_3:Fe_2O_3 films with cycle ratio 3:1 into a three-dimensionally configured substrate with the trench aspect ratio of 20:1.

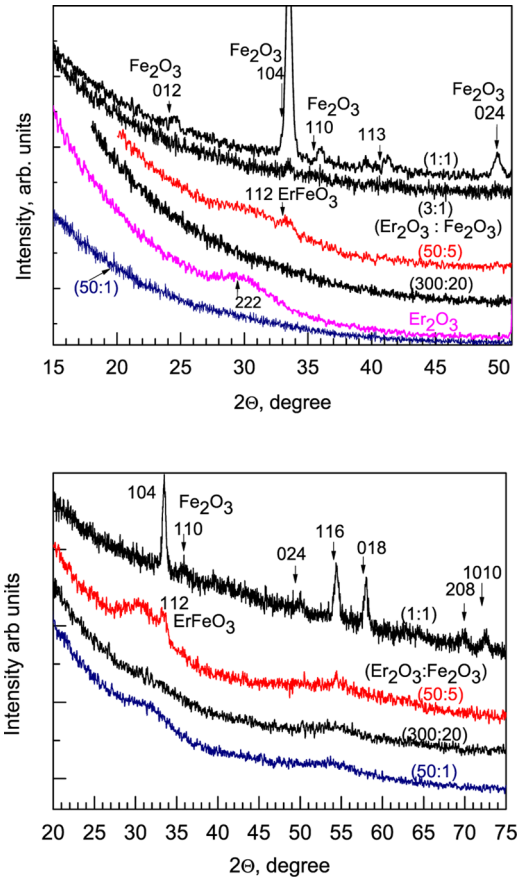

Figure 2. Grazing incidence X-ray diffraction (GIXRD) patterns of Er_2O_3:Fe_2O_3 films on SiO_2/Si substrate (upper panel), and on TiN/Si substrate (lower panel). Also shown is the pattern measured from the 4 nm thick reference Er_2O_3 film (upper panel). The cycle ratios (Er_2O_3:Fe_2O_3) are denoted by labels (see Table 1). The reflections are denoted with Miller indexes corresponding to hematite, cubic Er_2O_3, and orthorhombic $ErFeO_3$.

was grown to a relatively high thickness exceeding 50 nm using the Er_2O_3:Fe_2O_3 cycle ratios of 3:1 specifically to examine the possibility to grow oxides, using that particular precursor chemistry, onto three-dimensionally (3D) designed silicon-based substrates. As one can see in Figure 1, the film could be grown along the depth of ca. half micrometer in trenches build into a silicon wafer substrate with the aspect ratio 20:1, with certain amount of the growing material reaching the bottom of the trenches, although the nucleation of the solid layer was apparently not uniform throughout the whole depth.

X-ray diffraction studies on the films with very low Er content, i.e., on the films grown using Er_2O_3:Fe_2O_3 cycle ratios of 1:1 on SiO_2/Si, clearly revealed a crystal growth (Figure 2).

For this film, the reflections can be indexed considering only the rhombohedral hematite phase of iron oxide (PDF card 033-0664). One may actually consider also multiphase, more disordered, nature of the film with contribution from iron oxide phases with similar stoichiometry but different lattice, such as that of the hexagonal Fe_2O_3 with reflections 017, 116, and 204 at 24.6, 33.8, and 36.462°, respectively (PDF card 040-1139), which actually more precisely coincide with the centers of the gravity of the reflection peaks registered. Trace reflections from orthorhombic Fe_2O_3 with 020 at 36.191° (PDF card 047-1409) may be considered as well. However, it is worth noting that the same films grown on ca. 5 nm thick TiN layer (Figure 2) were also crystallized, whereas the locations of the reflections gave better fit with those of hematite. The iron-free Er_2O_3 film grown to the thickness of 4 nm was obviously not entirely amorphous but exhibited a nanocrystalline nature with a broad 222 peak around 29.5−30° (Figure 2). Small thickness of the film was evidently the main reason for the small size of crystallites leading to this kind of diffraction pattern. Further, the films grown with cycle ratios allowing larger, measurable, erbium-to-iron cation ratios occurred essentially amorphous. Exceptionally, the film grown with the Er_2O_3:Fe_2O_3 cycle ratio of 50:5 demonstrated a pattern with a broad peak at around 33.2°, which just may be attributed to the 112 reflection from $ErFeO_3$ (PDF card 047-0072), and thus allowing one to consider partial formation of the nanocrystalline erbium ferrite phase. The phase determination here remains ambiguous and, in fact, incomplete. The broad band formed between 30 and 35° in the diffractogram of the film grown with the cycle ratio of 50:5 allows one to consider the formation of a multiphase nanostructure and nucleation of iron-rich $ErFe_2O_4$ and/or $Er_2Fe_5O_{12}$ (ICPDS card 023-0240) phases. This may occur possibly also because of the excess of iron content in accord with the measured Er/Fe atomic ratio (see Table 1). The appearance of the latter iron-rich phases was considered possible also in the ALD-grown Er−Fe−O films earlier.[8]

DOI: 10.1021/acsomega.7b01394
ACS Omega 2017, 2, 8836−8842

Magnetic and Electric Behavior. Magnetic measurements were performed with the magnetic field applied in plane of the surface of the substrate for the Er_2O_3:Fe_2O_3 films. The structures demonstrated a ferromagnetic-like behavior at room temperature with saturation magnetization (Figure 3).

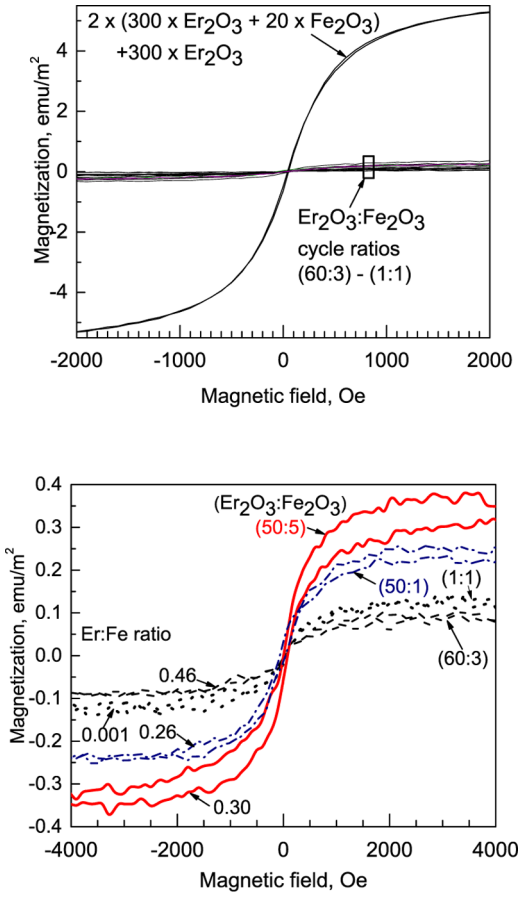

Figure 3. Representative magnetic moment vs external magnetic field strength curves measured from all of the Er_2O_3:Fe_2O_3 films deposited, as shown in the upper panel, whereas the lower panel represents the magnetization curves from films grown using relatively lower amounts of Er_2O_3 cycles, designated together with cycle ratios (60:3)−(1:1) in the upper panel, in a larger scale. For the film thicknesses, see Table 1.

One could see that the films containing Er_2O_3 and Fe_2O_3 layers deposited using relatively large amounts of growth cycles separately for constituent oxides, i.e., 300 cycles for Er_2O_3 and 20 cycles for Fe_2O_3, demonstrated a markedly stronger magnetization than the more homogeneously mixed Er−Fe−O films. The saturation magnetization in the film denoted with the cycle ratio (300:20) was 5.3 emu/m^2, i.e., 10 times higher than that in the mixed/doped Er_2O_3:Fe_2O_3 films, regardless of the lower thickness compared to that of the films with a more uniform distribution of erbium.

It is known that the magnetic properties of nanostructures can, besides chemical composition, markedly depend on defects, morphology, phase, and growth recipe. The magnetization in the composites or mixtures containing iron oxide could be enhanced by increasing the relative content of iron oxide in the materials deposited, as we have observed, for instance, in Bi_2O_3−Fe_3O_4 films grown by ALD[15] or Fe_3O_4−MgO by ALD.[16] It is likely that in our most strongly magnetized sample, the Fe_2O_3 interlayers, despite their X-ray amorphous nature, were still formed as stoichiometric iron oxides, although in a short-range order only, thereby giving the most prominent magnetic response in this sample series. It is to be noted that in $ErFeO_3$ films with a defined structure grown by pulsed laser deposition, certain magnetization-field hysteresis was registered at 130 K at the highest.[5] Further, in the films grown in the present study, the monotonic relationship between the Er/Fe cation ratio and the magnetization was not recognized (see Figure 3). The Er−Fe−O films deposited by ALD earlier[8] have demonstrated a somewhat analogous magnetization-field behavior with saturation magnetization not exceeding 30% from that of iron oxide. In the latter study, however, the coercivity was somewhat better defined, approaching 1 T.

In Figure 4, the capacitance−voltage curves measured from the metal−insulator−metal (MIM)-type capacitor structures are depicted.

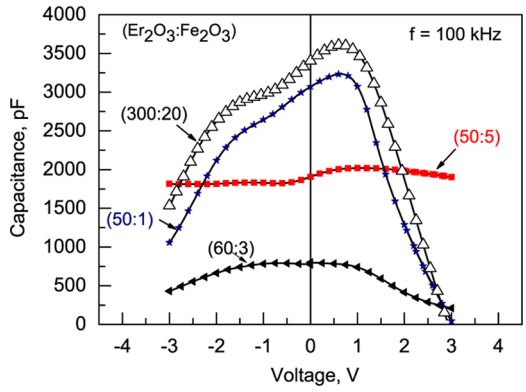

Figure 4. Capacitance−voltage curves of Al/Ti/Er_2O_3:Fe_2O_3/TiN/Ti/Si/Al capacitor structures containing Er_2O_3:Fe_2O_3 films deposited using constituent oxide cycle ratios indicated by labels, measured at 100 kHz.

The capacitance−voltage (C−V) curves are, in a satisfactory approximation, characteristic of those commonly seen with metal−insulator−metal (MIM)-like structures with quite leaky dielectric layers, i.e., with certain plateau tending to appear around zero bias voltages, and further deviations in the effective capacitance with increase in the absolute bias values.[17−19] In the present case, the decrement of capacitance at larger biases is obvious, especially in the films with relatively low thicknesses, i.e., those grown with the cycle ratios 300:20, 60:3, or 50:1. One can propose that capacitance is influenced, besides the major affections from the film thickness and permittivity, also by the conductivity of the films, enabling leakage of charge carriers. Charge accumulation at two-dimensional defect layers caused by the deposition of small amounts or Er_2O_3 embedded in Fe_2O_3, as well as at the electrode−film interfaces, is possible reason for this influence. Indeed, separate measurements carried out to record the conductance of the materials against the bias voltage revealed that the curves built up on values approximately reciprocal to those of the capacitance (Figure 5).

It is thus likely that the decrement of the capacitance at higher biases is due to the formation of double (multiple) capacitances in series throughout the layered stack of oxides, together with their interfaces to electrodes, as well as possibly, at the barriers in the "bulk" of oxide films consisting of layers with variable structure and chemical composition. The variations may arise already from the nature of ALD proceeding

DOI: 10.1021/acsomega.7b01394
ACS Omega 2017, 2, 8836−8842

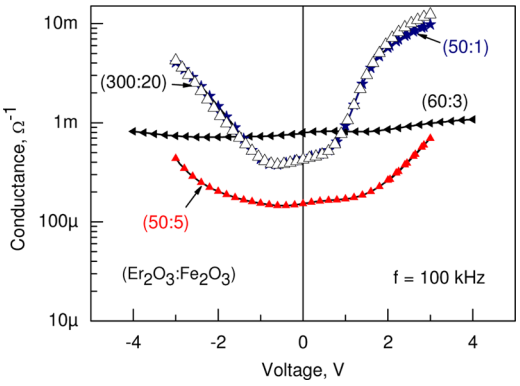

Figure 5. Conductance–voltage curves of Al/Ti/Er_2O_3:Fe_2O_3/TiN/Ti/Si/Al capacitor structures containing Er_2O_3:Fe_2O_3 films deposited using constituent oxide cycle ratios indicated by labels, measured at 100 kHz.

via a sequential deposition of the constituent compound materials.

Assuming that the oxide film does form the thickest part of capacitive stack of layers and thus dominates in the series of capacitors, it is still possible to roughly estimate the average permittivity of the oxide-based films, taking into account the capacitance values recorded under alternating current component of the applied voltage at zero bias. The relative permittivity of the stacked material can then simply be calculated taking into account the parallel-plate capacitor model. It is thereby also to be considered that the permittivity calculated in this manner does not reflect the physical property of the metal oxide layer alone, but it is deviated by the charge-polarized and concurrent fields built up at the interface layers. Therefore, the permittivity calculated from the capacitance measured must be lower than the one truly characteristic of the metal oxide layer, and the detrimental effect of the interfaces must increase with decrease in film thickness. Nevertheless, the estimated permittivities for the 5, 19.5, and 14.9 nm thick films grown using the cycle ratios of 300:20, 50:5, and 50:1 (see Figure 5) were as high as 9.4, 20.6, and 25.3, respectively, at zero bias and 100 kHz. In these films, the relative content of erbium was high enough to allow at least partial formation of the iron-rich ferrite phases (see Figure 2). Of course, one cannot exclude the interference of leakage, as was noted above, which may, as opposed to the effect of interface layers, give rise to the apparent capacitance as measured. Further, the permittivity of the amorphous 5.2 nm thick film grown with the cycle ratio of 60:3 was only 2.3. Note, that the estimations were made without the corrections taking account the likely effects of interfacial layers and series capacitances inevitably affecting the total capacitance values.

Regarding the literature data, polycrystalline hematite α-Fe_2O_3 has demonstrated the relative permittivity close to unity or even lower[20,21] at frequencies close to 100 kHz used in the present study. The ternary compounds of erbium, iron, and oxygen would exhibit a markedly higher permittivity. Polycrystalline $ErFeO_3$ ceramics have been described as materials possessing permittivity values exceeding 60 at 2 kHz.[22] Both polycrystalline[23] and single-crystalline[24] $ErFe_2O_4$ have been characterized as materials with a large dielectric constant in the order of 10^4. In the present study, the calculated permittivity may thus indeed be partially influenced by the phase composition of oxide films, being higher in the films in which short-range order may resemble that of orthoferrites and lower in the films with major contribution from crystalline hematite, in addition to the amorphous parts and interfaces.

The films grown demonstrated noticeable leakage currents, as can be seen in Figure 6. Although the dielectric breakdown

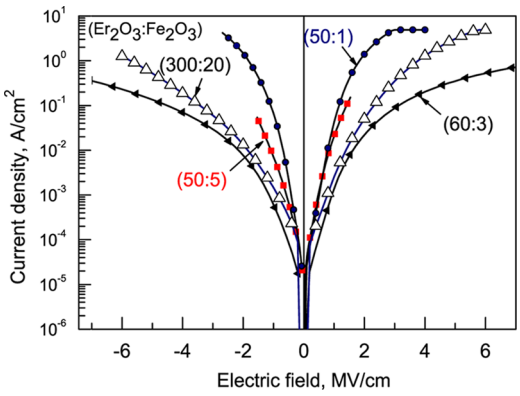

Figure 6. Leakage current–field curves of Al/Ti/Er_2O_3:Fe_2O_3/TiN/Ti/Si/Al capacitor structures containing Er_2O_3:Fe_2O_3 films deposited using constituent oxide cycle ratios indicated by labels. For the sample thicknesses and composition, see Table 1.

in the films was not observed, the currents increased rapidly with the applied voltage under the electric fields ranging over few MV/cm. One could expectedly obtain a relatively lower leakage in the mainly amorphous films. In general, it is evident that the currents through the stacks are to be considered as factors able to affect the charge polarization at the layer interfaces.

Polarization charge vs applied voltage (P–V) characteristics measured on Al/Ti/Er_2O_3:Fe_2O_3/TiN/Ti/Si/Al structures in Sawyer–Tower circuit are shown in Figure 7.

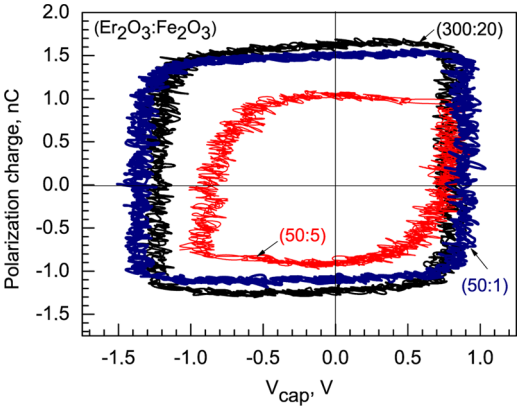

Figure 7. Polarization charge vs voltage applied to the capacitive elements in Sawyer–Tower circuit for Er_2O_3:Fe_2O_3 films with cycle ratios denoted by labels.

One can see that the samples fabricated with cycle ratios 300:20, 50:5, and 50:1 exhibited a certain, rather quadratic, hysteresis loop (Figure 7, upper panel) and the films possessed charge polarization measured at room temperature.

One can also see that the charge polarization does not quite proceed in the form of the classical hysteresis loop characterizing ferroelectric materials, as there is no defined plateau apparent in polarized charge against increasing voltage (field). Quite likely, significant amount of the charge, responsible for

DOI: 10.1021/acsomega.7b01394
ACS Omega 2017, 2, 8836–8842

the effectively measurable polarization in the material deposited, is drifting in the material under external field and becomes trapped at the interfaces between metal oxide and the electrode layers, causing interfacial polarization. Consequently, the electrical charge becomes carried to and trapped at the interface layer under certain polarity, and an opposite polarity with increasing, oppositely directed, field is required to release the charge from the traps, which is the main cause for the apparently spontaneous charge polarization between 0.8 and 1.8 nC over an electrode with an area of 0.024 mm^2. On the other hand, somewhat analogous polarization-field behavior has been observed and recorded for pulsed laser-deposited hexagonally structured $ErFeO_3$ films[4,5] and, together with magnetization behavior, was designated as a signature of the multiferroic performance of that material.

CONCLUSIONS

In summary, the atomic layer deposition of Er_2O_3:Fe_2O_3 thin films with Er/Fe atomic ratios up to 0.46 was realized. All of the samples exhibited saturation magnetization and charge polarization measured at room temperature. Promising results in terms of the simultaneous appearance of internal magnetization and certain electrical charge polarization were demonstrated in planar Er_2O_3:Fe_2O_3 structures. Further electrical and magnetic modeling and analysis will be needed to elaborate the phenomenon and optimize the material structure for magnetoelectric performance.

EXPERIMENTAL SECTION

The films were deposited in a flow-type in-house built hot-wall ALD reactor[25] using $Er(thd)_3$ and $FeCp_2$ as metal precursors and O_3 as an oxygen precursor. N_2 (99.999%) was used as the carrier and purge gas. In all of the cases, an ALD cycle was started with a metal precursor pulse and continued with a purge of the reaction zone with pure carrier gas, followed by oxygen precursor pulse and another purge. To obtain sufficient precursor pressures, the $Er(thd)_3$ source temperature was set at 160 °C and $FeCp_2$ source was set at 60 °C. The Er_2O_3:Fe_2O_3 films and laminate structures were grown at 375 °C by applying certain numbers of constituent binary oxide growth cycles alternately (Table 1). The cycle times were 5−5−5−5 s for the sequence of metal precursor pulse−purge−ozone pulse−purge. To obtain films with different composition starting with very light doping and ending with almost laminated structures, the ratio of the cycle numbers used for the deposition of Er_2O_3 and Fe_2O_3 was varied keeping the total number of cycles approximately at the same level for all of the samples. The substrate temperature of 375 °C was chosen to achieve appreciable compromise between the temperatures suited to both metal precursors. β-Diketonates are expected to decompose thermally rather intensely at 400 °C and higher temperatures, whereas the reactivity of ferrocene and, concurrently, the growth rate of iron oxide would decrease notably with the decrease in substrate temperature below 350 °C.

The mass thickness and elemental composition of the films were measured by X-ray fluorescence spectroscopy method using ZSX400 (Rigaku) spectrometer. For the calibration of the measurement procedure, we used binary Er_2O_3 and Fe_2O_3 films with known thicknesses and densities determined by the X-ray reflection (XRR) method. Grazing incidence X-ray diffraction (GIXRD) was applied for structural studies, and all of the XRD and XRR studies were carried out with Smartlab (Rigaku) X-ray analyzer using Cu Kα radiation. In addition, thicknesses of a series of films with different compositions were determined using GES5E (Sopra-Semilab) spectroscopic ellipsometer. The morphology of nanostructures on the Si substrate and on three-dimensional (3D) substrates were investigated by scanning electron microscopy (SEM) using a Dual BeamVR equipment Helios NanoLab 600 (FEI) equipped with a focused ion beam (FIB) module. The FIB was employed for the preparation of samples on the 3D-configured substrate stack.

The films grown on Si substrates (Table 1) were subjected to magnetic measurements. The measurements were performed by using a vibrating sample magnetometer option of a physical property measurement system 14 T (Quantum Design). Rectangular samples with dimensions of around 5 × 4 mm^2 were fixed with general electric varnish on the commercial quartz sample holders (Quantum Design). The magnetization was measured at room temperature (350 K) and in the presence of a magnetic field of 79.6 kA/m parallel to the film surface. Magnetization isotherms were measured by scanning the magnetic fields from −4800 to +4800 kA/m. The films subjected to magnetometry were grown on nondoped silicon also without an additional TiN electrode layer. This was to avoid possible interferences by magnetization signal and noise from the substrates. The diamagnetic signal arising from the pure silicon substrate was subtracted from the general magnetization curve for all of the samples in which ferromagnetic-like response was detected.

To carry out the electrical measurements, metal−insulator−metal (MIM) structures were prepared. Silicon substrates with 5 nm thick TiN layers grown by chemical vapor deposition were used as bottom electrodes. Top electrodes with an area of 0.204 mm^2 were formed by the electron beam evaporation of 30 nm thick Ti layers directly in contact with Er−Fe−O film, followed by the evaporation of 120 nm thick Al on Ti through a shadow mask. The electrical characterization techniques used were capacitance−voltage ($C-V$) and current−voltage ($I-V$) measurements. The electrical measurements were done by means of an Agilent DXO-X 3104 digital oscilloscope with a built-in wave generator. The standard Sawyer−Tower experiment was carried out by applying a periodic triangular stimulus and recording the voltage loops data from the oscilloscope. The charge values were obtained from the sensed voltage across a stated capacitance.

AUTHOR INFORMATION

Corresponding Author

*E-mail: aile.tamm@ut.ee.

ORCID

Aile Tamm: 0000-0002-0547-0824

Notes

The authors declare no competing financial interest.

ACKNOWLEDGMENTS

This work was supported, partially, by the European Regional Development Fund project TK134 “Emerging orders in quantum and nanomaterials”, Estonian Ministry of Education and Research (IUT2-24), Estonian Academy of Sciences (SLTFYUPROF), and Spanish Ministry of Economy and Competitiveness through the project TEC2014-52152-C3-3-R with support of Feder funds.

DOI: 10.1021/acsomega.7b01394
ACS Omega 2017, 2, 8836−8842

REFERENCES

(1) Jeong, Y. K.; Lee, J.-H.; Ahn, S.-J.; Song, S.-W.; Jang, H. M.; Choi, H.; Scott, J. F. Structurally tailored hexagonal ferroelectricity and multiferroism in epitaxial $YbFeO_3$ thin-film heterostructures. *J. Am. Chem. Soc.* **2012**, *134*, 1450.

(2) Wang, W.; Zhao, J.; Wang, W.; Gai, Z.; Balke, N.; Chi, M.; Lee, H. N.; Tian, W.; Zhu, L.; Cheng, X.; Keavney, D. J.; Yi, J.; Ward, T. Z.; Snijders, P. C.; Christen, H. M.; Wu, W.; Shen, J.; Xu, X. Room-temperature multiferroic hexagonal $LuFeO_3$ films. *Phys. Rev. Lett.* **2013**, *110*, No. 237601.

(3) Akbashev, A. R.; Semisalova, A. S.; Perov, N. S.; Kaul, A. R. Weak ferromagnetism in hexagonal orthoferrites $RFeO_3$ (R = Lu, Er−Tb). *Appl. Phys. Lett.* **2011**, *99*, No. 122502.

(4) Yokota, H.; Nozue, T.; Nakamura, S.; Fukunaga, M.; Fuwa, A. Examination of ferroelectric and magnetic properties of hexagonal $ErFeO_3$ thin films. *Jpn. J. Appl. Phys.* **2015**, *54*, No. 10NA10.

(5) Yokota, H.; Nozue, T.; Nakamura, S.; Hojo, H.; Fukunaga, M.; Janolin, P.-E.; Kiat, J.-M.; Fuwa, A. Ferroelectricity and weak ferromagnetism of hexagonal $ErFeO_3$ thin films. *Phys. Rev. B* **2015**, *92*, No. 054101.

(6) Sivakumar, M.; Gedanken, A.; Bhattacharya, D.; Brukental, I.; Yeshurun, Y.; Zhong, W.; Du, Y. W.; Felner, I.; Nowik, I. Sonochemical synthesis of nanocrystalline rare earth orthoferrites using $Fe(CO)_5$ precursor. *Chem. Mater.* **2004**, *16*, 3623−3632.

(7) Koohpayeh, S. M.; Abell, J. S.; Bamzai, K. K.; Bevan, A. I.; Fort, D.; Williams, A. J. The influence of growth rate on the microstructural and magnetic properties of float-zone grown $ErFeO_3$ crystals. *J. Magn. Magn. Mater.* **2007**, *309*, 119−125.

(8) Mantovan, R.; Vangelista, S.; Wiemer, C.; Lamperti, A.; Tallarida, G.; Chikoidze, E.; Dumont, Y.; Fanciulli, M. Synthesis of multiferroic Er-Fe-O thin films by atomic layer and chemical vapor deposition. *J. Appl. Phys.* **2014**, *115*, No. 17D907.

(9) Vangelista, S.; Lamperti, A.; Wiemer, C.; Fanciulli, M.; Mantovan, R. Atomic layer deposition of hexagonal $ErFeO_3$ thin films on SiO_2/Si. *Thin Solid Films* **2016**, *604*, 18−22.

(10) Martinson, A. B. F.; DeVries, M. J.; Libera, J. A.; Christensen, S. T.; Hupp, J. T.; Pellin, M. J.; Elam, J. W. Atomic layer deposition of Fe_2O_3 using ferrocene and ozone. *J. Phys. Chem. C* **2011**, *115*, 4333.

(11) Zierold, R.; Le Lam, C.; Dendooven, J.; Gooth, J.; Böhnert, T.; Sergelius, P.; Munnik, F.; Moreno, J. M. M.; Görlitz, D.; Detavernier, C.; Nielsch, K. Magnetic characterization and electrical field-induced switching of magnetite thin films synthesized by atomic layer deposition and subsequent thermal reduction. *J. Phys. D: Appl. Phys.* **2014**, *47*, No. 485001.

(12) Rooth, M.; Johansson, A.; Kukli, K.; Aarik, J.; Boman, M.; Hårsta, A. Atomic layer deposition of iron oxide thin films and nanotubes using ferrocene and oxygen as precursors. *Chem. Vap. Deposition* **2008**, *14*, 67.

(13) Tamm, A.; Dimri, M. C.; Kozlova, J.; Aidla, A.; Tätte, T.; Arroval, T.; Mäeorg, U.; Mändar, H.; Stern, R.; Kukli, K. Atomic layer deposition of ferromagnetic iron oxide films on three-dimensional substrates with tin oxide nanoparticles. *J. Cryst. Growth* **2012**, *343*, 21−27.

(14) Päiväsaari, J.; Putkonen, M.; Niinistö, L. A comparative study on lanthanide oxide thin films grown by atomic layer deposition. *Thin Solid Films* **2005**, *472*, 275.

(15) Puttaswamy, M.; Vehkamäki, M.; Kukli, K.; Dimri, M. C.; Kemell, M.; Hatanpää, T.; Heikkilä, M. J.; Mizohata, K.; Stern, R.; Ritala, M.; Leskelä, M. Bismuth iron oxide thin films using atomic layer deposition of alternating bismuth oxide and iron oxide layers. *Thin Solid Films* **2016**, *611*, 78−87.

(16) Kukli, K.; Dimri, M. C.; Tamm, A.; Kemell, M.; Käämbre, T.; Vehkamäki, M.; Puttaswamy, M.; Stern, R.; Kuusik, I.; Kikas, A.; Tallarida, M.; Schmeißer, D.; Ritala, M.; Leskelä, M. Structural and magnetic studies on iron oxide and iron-magnesium oxide thin films deposited using ferrocene and (dimethylaminomethyl)ferrocene precursors. *ECS J. Solid State Sci. Technol.* **2013**, *2*, N45−N54.

(17) Wenger, C.; Lupina, G.; Lukosius, M.; Seifarth, O.; Müssig, H.-J.; Pasko, S.; Lohe, C. Microscopic model for the nonlinear behavior of high-k metal−insulator−metal capacitors. *J. Appl. Phys.* **2008**, *103*, No. 104103.

(18) Kannadassan, D.; Karthik, R.; Baghini, M. S.; Mallick, P. S. Modeling the voltage nonlinearity of high-k MIM capacitors. *Solid-State Electron.* **2014**, *91*, 112−117.

(19) Austin, D. Z.; Holden, K. E. K.; Hinz, J.; Conley, J. F., Jr. Electrode modulated capacitance-electric field nonlinearity in metal-insulator-metal capacitors. *Appl. Phys. Lett.* **2017**, *110*, No. 263503.

(20) Papaioannou, J. C.; Patermarakis, G. S.; Karayianni, H. S. Electron hopping mechanism in hematite (α-Fe_2O_3). *J. Phys. Chem. Solids* **2005**, *66*, 839−844.

(21) Shinde, S. S.; Bansode, R. A.; Bhosale, C. H.; Rajpure, K. Y. Physical properties of hematite α-Fe_2O_3 thin films: application to photoelectrochemical solar cells. *J. Semicond.* **2011**, *32*, No. 013001.

(22) Ye, J. L.; Wang, C. C.; Ni, W.; Sun, X. H. Dielectric properties of $ErFeO_3$ ceramics over a broad temperature range. *J. Alloys Compd.* **2014**, *617*, 850−854.

(23) Ikeda, N.; Kohn, K.; Kito, H.; Akimitsu, J.; Siratori, K. Dielectric relaxation and hopping of electrons in $ErFe_2O_4$. *J. Phys. Soc. Jpn.* **1994**, *63*, 4556−4564.

(24) Ikeda, N.; Kohn, K.; Kito, H.; Akimitsu, J.; Siratori, K. Anisotropy of dielectric dispersion in $ErFe_2O_4$ single crystal. *J. Phys. Soc. Jpn.* **1995**, *64*, 1371−1377.

(25) Arroval, T.; Aarik, L.; Rammula, R.; Kruusla, V.; Aarik, J. Effect of substrate-enhanced and inhibited growth on atomic layer deposition and properties of aluminum−titanium oxide films. *Thin Solid Films* **2016**, *600*, 119−125.

DOI: 10.1021/acsomega.7b01394
ACS Omega 2017, 2, 8836−8842